Scaling theory for two-dimensional systems with competing interactions

Antitsa D. Stoycheva and Sherwin J. Singer
Department of Chemistry, Ohio State University, 100 West 18th Avenue, Columbus, Ohio 43210
(Received 22 January 2001; published 20 June 2001)

We derive an analytic scaling theory for a two-dimensional system in which spontaneous patterns of stripes, bubbles, and intermediately shaped domains arise due to the competition of short-range attractions and long-range dipolar repulsions. The theory predicts temperature and domain-size scaling as a function of the relative repulsion strength η, the ratio of the repulsive to the attractive coupling constant in the system's Hamiltonian. As η decreases, the domain size explodes exponentially and the melting temperature for a system of ordered stripes increases. Our findings shed new light on the phase diagram and critical excitations for the dipolar Ising ferromagnet or lattice gas and their continuum analogs. We show that the features described by the scaling theory are insensitive to details like cutoffs for the dipolar interactions and, therefore, should be widely applicable. Our corresponding states analysis explains the experimentally observed stripe melting upon compression in a Langmuir monolayer. A phenomenological extension of the analytic scaling theory describes how the system's behavior is modified in the presence of magnetization or density fluctuations. Fluctuations are found to suppress domain size and the stripe melting temperature. In regimes where fluctuations are important, we predict that domain size will decrease with increasing temperature.

DOI: 10.1103/PhysRevE.64.016118 PACS number(s): 05.65.+b, 89.75.Kd, 05.50.+q, 68.55.−a

I. INTRODUCTION

A variety of two- and three-dimensional systems with competing attractive and repulsive interactions self-organize into patterns of stripes, bubbles, and domains of intermediate shapes [1]. Examples of spontaneously modulated materials range from ferromagnetic and dielectric compounds [2,3] through Langmuir monolayers [1,4–9] to adsorbed monolayers on solid surfaces [10–13]. The bubbles, stripes, and other patterns observed in these materials have been the object of many experimental and theoretical studies. These materials form the basis of several promising technologies. For example, either by direct assembly on a substrate or by transfer from a Langmuir phase, self-assembled monolayers have recently been demonstrated to be a feasible route to the fabrication of surface nanoscale devices [14–17].

The occurrence of similar spatial patterns across a wide variety of physical systems has been attributed to a common mechanism, the competition of short-range attractive forces and long-range repulsions [1,9,18]. The long-range repulsions have been found to be due to actual or effective dipoles whose interaction energy falls off as r^{-3} with distance, although in two dimensions the precise form of the repulsive interaction might not be crucial. Magnetostatic interactions between spins produce the dipolar repulsion between domains in thin ferromagnetic films [2,3]. Surface polarization is the source of the repulsion in Langmuir monolayers. [5–9,19,20] Either surface polarization or accumulation of elastic energy from lattice mismatch cause actual or effective dipolar repulsion within adsorbed monolayers on solid substrates [21–23]. In most cases the domain length scale is much longer than a molecular one. Therefore, domain formation on the mesoscopic level is controlled by a few materials parameters and the molecular details of the system recede in importance.

We denote the attractive and repulsive interaction parameters by J and A, respectively. The fundamental question we answer in this paper is the following (see Fig. 1): If a set of interaction parameters J and A gives rise to domains with a particular length scale, is there another set of parameters $J(b)$ and $A(b)$ that gives rise to the same domain configurations as the original parameters, only scaled in size by a factor b? The answer turns out to be affirmative under a broad range of conditions. The availability of this type of ''corresponding states'' theory provides valuable information about systems with a highly complex phase diagram and can be tested experimentally, as described below.

Although a body of analytic theory [19,24–28] and numerical simulations [29–31] treating modulated phases has accumulated, the phase diagram and the elementary excitations leading to phase transitions in these systems have not been completely elucidated. We have recently presented a brief report [32] of large-scale numerical simulations of stripe phase melting in an Ising model with additional long-range dipolar repulsive interactions, one of the basic models for modulated phases that are stabilized by competing attractions and repulsions. By ''melting'' of stripe phases we

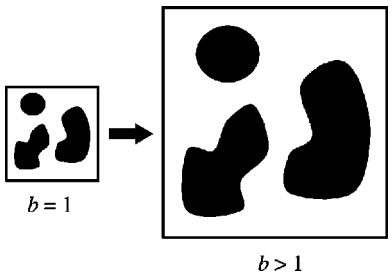

FIG. 1. Two configurations are shown, the original configuration of domains ($b=1$) and another configuration that is identical to the original except that the domains are scaled in size by a factor b. ($b>1$ is shown here.) The original system configuration is specified by a set of domain areas $\{\mathcal{D}_i\}$ and contours $\{\mathcal{C}_i\}$. The areas and contours of the scaled domains are indicated by $\{b\mathcal{D}_i\}$ and $\{b\mathcal{C}_i\}$, respectively.

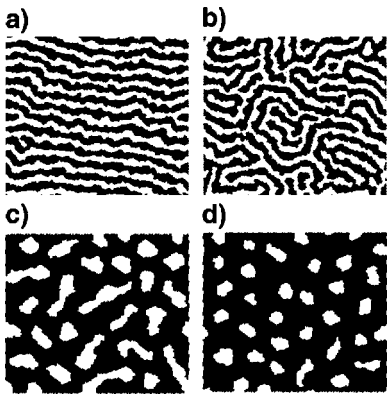

FIG. 2. Representative snapshots from Monte Carlo simulations [32,52] of the dipolar Ising model [Eq. (1)]. (a) Stripe phase; (b) isotropic phase, ''melted'' stripes; (c) isotropic phase, elongated bubble domains; (d) isotropic phase, bubble domains.

mean loss of the twofold orientational order of the stripe phase [Fig. 2(a)] to either a meandering stripe phase [Fig. 2(b)] or a bubble phase [Figs. 2(c) and 2(d)]. (In two dimensions, the stripe phase does not have true long-ranged orientational order. Rather, the decay of orientational correlations switches between algebraic and exponential character at the transition point [25].) Our work established that, for sufficiently large values of the relative repulsion strength A/J, the stripe phase disorders via topological defects and, most likely, is an instance of Kosterlitz-Thouless topological defect unbinding [33–37]. Our simulations revealed a clear trend in which the stripe melting temperature increased as the ratio A/J decreased. The data from simulations were found to be in agreement with a preliminary version of the scaling theory, which was presented in our brief report without derivation [32]. In this work, a more general and complete version of the scaling theory is derived. As discussed further below, the dependence of the stripe melting temperature on the ratio A/J, predicted by our scaling theory, explains an otherwise puzzling feature exhibited by stripe domains in Langmuir monolayers, namely, the fact that they disorder upon compression [38].

The basic model for modulated phases stabilized by dipolar repulsions is introduced in Sec. II, and a family of different short-range cutoffs for the dipolar interaction is introduced. For domains in which the radius of curvature is much larger than a microscopic cutoff length, we can treat the various cutoffs in a unified fashion, exposing possible effects due to the choice of a cutoff. In Sec. III, scaling relations are developed for the case in which domain boundaries are sharp and the density within domains does not change appreciably with temperature. In other words, we treat the case in which the domain shapes fluctuate, but not the density within domains. Readers not interested in the derivations given in Sec. III can proceed directly to Sec. IV, where we present the predictions of the scaling relations. Finally, in a highly phenomenological manner, we explore the case in which the domain densities also change in Sec. V. Those not interested in the derivation of Sec. V A may find the resulting predictions presented in Sec. V B. Conclusions are given in Sec. VI.

II. MODELS FOR MODULATED PHASES ARISING FROM DIPOLAR INTERACTIONS

In typical self-organizing systems of interest, domain length scales are much larger than atomic or molecular dimensions. Many details of the interaction are not important on the mesoscopic level, and we concentrate on the fundamental ingredients that are required to support modulated phases, a short-range attraction and a longer-ranged repulsion. We take the repulsion to be that between parallel dipoles, falling off as the third power of distance, because it is appropriate for both thin ferromagnetic films and Langmuir monolayers. We consider both continuum and lattice models. Continuum models are most amenable to analytic theory, including the scaling theory developed in this work. It is important to also consider lattice models, so that we can make connections between analytic theory and computer simulations, which are usually performed using lattice models (not to say that lattice models are without use in analytic theory). We actually begin with lattice models, where microscopic cutoffs arise naturally.

A. Spin and lattice gas Hamiltonians

Lattice models may be represented using either spin variables ($s_R = \pm 1$) or particle occupation variables ($n_R = 0,1$). It is well known that the two representations are equivalent and related to each other by the transformation $s_R = 2n_R - 1$. Since there are experimental realizations of modulated phases stabilized by dipole repulsions that correspond to both spin and occupation variables, we introduce the lattice Hamiltonian using both Ising-like spin variables ($\mathcal{H}_{Is}$),

$$\mathcal{H}_{Is}/k_BT = -J' \sum_{\langle R,R' \rangle} s_R s_{R'} + \frac{A'}{2} \sum_{R,R'} \frac{s_R s_{R'}}{|R-R'|^3} - h \sum_R s_R , \tag{1}$$

and lattice gas occupation variables ($\mathcal{H}_{LG}$),

$$\mathcal{H}_{LG}/k_BT = -J \sum_{\langle R,R' \rangle} n_R n_{R'} + \frac{A}{2} \sum_{R,R'} \frac{n_R n_{R'}}{|R-R'|^3} - \mu \sum_R n_R . \tag{2}$$

J' and J are attractive coupling constants, A' and A are the dipolar repulsive coupling constants in the lattice gas and spin representation, respectively, h is an external magnetic field, and μ is the chemical potential. The first term in Eqs. (1) and (2) captures the effect of short-range attractive interactions, the second one introduces long-range repulsions, and the third takes into account the influence of an external field or the chemical potential.

The well-known relations between coupling constants in the two representations are easily derived by substituting $s_R = 2n_R - 1$ into Eq. (1) and comparing with Eq. (2),

$$J = 4J', \tag{3}$$

$$A = 4A', \tag{4}$$

$$\mu \equiv \mu_0 + \delta\mu, \tag{5}$$

$$\mu_0 = 2\left(\frac{C_3}{a^3}A' - qJ'\right), \tag{6}$$

$$\delta\mu = 2h. \tag{7}$$

In Eq. (6),

$$C_3 = \sum_{R'(R'\neq R)} \frac{a^3}{|R-R'|^3}, \tag{8}$$

where a is the nearest-neighbor distance of the lattice. C_3 has the numerical value of 9.033 621 7 for a square lattice and 11.034 175 7 for a triangular lattice [27]. Physically, C_3 is the dimensionless interaction strength of a dipole at site R with an infinite two-dimensional array of parallel dipoles. q is the number of nearest neighbors for a particle at site R on the lattice.

B. Continuum limit: Pure domain shape fluctuations

We now proceed to the continuum limit. In this section, we suppose that system fluctuations are dominated by changes in domain shapes and not the density (or magnetization for spin systems) within domains. This condition is very well satisfied for values of A and J where it is feasible to perform simulations for an Ising model with dipolar repulsions (see Fig. 2), such as the model governed by Eq. (1). As will emerge from the theory below, the domain length scale increases faster than exponentially as the ratio A/J decreases. Therefore, beyond certain values of A/J, the domain length scale becomes larger than any practical simulation size. In the workable range of A/J, the stripe melting temperature is between five and ten times smaller than the critical temperature of the bare (without repulsions) Ising model [29,32]. As a result, nearly all spins have the same orientation and the density or magnetization is constant within each domain. To be fully convinced of this effect, the reader is urged to consult our numerical simulation results [29,32] or view animations from our simulations available electronically [39]. Experimentally, it also appears that in many instances domain shapes fluctuate while their density is nearly fixed, although typically these data are not reported. We explore the interesting case of density variations *within* the domains in Sec. V.

We use the symbols $\mathcal{D}_i$ to indicate the area and $\mathcal{C}_i$ for the contour of domain i. These are the effective degrees of freedom when density is fixed within domains and only domain shapes fluctuate. It is most convenient to approach the continuum limit using the lattice gas Hamiltonian of Eq. (2). The contribution from attractive interactions within a domain is written as a bulk plus a surface term,

$$-J\sum_{\langle R,R'\rangle} n_R n_{R'} \approx -\sum_i J\frac{q}{2\sigma}\int_{\mathcal{D}_i} d\mathbf{r} + \sum_i J\gamma\int_{\mathcal{C}_i} dl, \tag{9}$$

where σ is the area per lattice site, dl is an element of arc length, and $J\gamma$ is the line tension. The factor γ times a microscopic length, like the lattice constant, is a number of order unity. Estimates of γ at 0 K are provided in Ref. [27].

After the terms involving long-range repulsions are taken to the continuum limit by turning sums over lattice sites R into integrals, we obtain the following continuum Hamiltonian:

$$\begin{aligned}\mathcal{H}_{LG}/k_BT = &-\left[\mu + \frac{q}{2}J\right]\frac{1}{\sigma}\sum_i \int_{\mathcal{D}_i} d\mathbf{r} + \gamma J\sum_i \int_{\mathcal{C}_i} dl \\ &+ \sum_{i<j}\frac{A}{\sigma^2}\int_{\mathcal{D}_i}\int_{\mathcal{D}_j} d\mathbf{r}d\mathbf{r}' v(|\mathbf{r}-\mathbf{r}'|) \\ &+ \sum_i \frac{A}{2\sigma^2}\int_{\mathcal{D}_i}\int_{\mathcal{D}_i} d\mathbf{r}d\mathbf{r}' v(|\mathbf{r}-\mathbf{r}'|).\end{aligned} \tag{10}$$

The interdomain and intradomain dipolar repulsion energies are separated in the above equation because they will be treated in a different manner below. They both contain the repulsive interaction potential function $v(|\mathbf{r}-\mathbf{r}'|)$, which approaches $|\mathbf{r}-\mathbf{r}'|^{-3}$ as $|\mathbf{r}-\mathbf{r}'|\to\infty$. In the continuum limit, the $|\mathbf{r}-\mathbf{r}'|^{-3}$ repulsion between point dipoles must be cut off at short range to avoid unphysical divergences. Realistically, the interaction is cut off because dipoles are really finite and not point dipoles, or polar molecules never get closer than a certain distance because of excluded volume interactions. Various model calculations have incorporated a short-range cutoff in different ways. Some use an explicit finite-dipole interaction [40,41]. Others impose a distance of closest approach either by virtue of working on a lattice [27,28,42] or by additional hard disk or hard sphere interactions for continuous two- [27,28,43] and three- [44–47] dimensional systems. To treat the various cutoff functions in a unified manner, we define a general cutoff function $w(r)$ and cutoff distance $a(a\sim\sqrt{\sigma})$ such that

$$v(r) = w\left(\frac{r}{a}\right)r^{-3}, \tag{11}$$

where $w(r/a)\to 1$ when $r\gg a$, and $w(r/a)$ decreases sufficiently rapidly as $r\to 0$, to ensure that the integrals over the dipolar repulsion energy in Eq. (10) remain finite. Without loss of generality, we take the domains to be the minority phase and what lies between domains to be the majority phase. In this case the average separation between domains is comparable to the domain length scale (e.g., stripe width or bubble diameter) near half coverage, and greater than this distance at less than half coverage. Since domains are thus separated by large distances compared to the cutoff a, we may set $w(|\mathbf{r}-\mathbf{r}'|/a)=1$ in the interdomain energy term. With the substitution of Eq. (11) into Eq. (10) and taking $w(|\mathbf{r}-\mathbf{r}'|/a)=1$ in the interdomain repulsion term, the lattice gas Hamiltonian becomes

$$\begin{aligned}\mathcal{H}_{LG}/k_BT = &-\left[\mu + \frac{q}{2}J\right]\frac{1}{\sigma}\sum_i \int_{\mathcal{D}_i} d\mathbf{r} + \gamma J\sum_i \int_{\mathcal{C}_i} dl \\ &+ \sum_{i<j}\frac{A}{\sigma^2}\int_{\mathcal{D}_i}\int_{\mathcal{D}_j} d\mathbf{r}d\mathbf{r}'|\mathbf{r}-\mathbf{r}'|^{-3} \\ &+ \sum_i \frac{A}{2\sigma^2}\int_{\mathcal{D}_i}\int_{\mathcal{D}_i} d\mathbf{r}d\mathbf{r}' w\left(\frac{|\mathbf{r}-\mathbf{r}'|}{a}\right)|\mathbf{r}-\mathbf{r}'|^{-3}.\end{aligned} \tag{12}$$

C. Cutoff functions

To gauge how the choice of cutoff for the dipole interactions [see Eq. (11)] affects the scaling properties, several cutoffs that have been used previously in the literature (the citations are by no means exhaustive) and other reasonable forms are given here. We have enforced a similar normalization for all the choices: $v(r)\to r^{-3}$ and $w(r/a)\to 1$ as $r\to\infty$.

(1) Sharp cutoff [27,28,42]

$$w\left(\frac{r}{a}\right)=\theta\left(\frac{r}{a}-1\right)=\begin{cases}0, & r<a\\ 1, & r>a,\end{cases} \tag{13}$$

$$v(r)=\theta\left(\frac{r}{a}-1\right)r^{-3}=\begin{cases}0, & r<a\\ r^{-3}, & r>a.\end{cases} \tag{14}$$

(2) Finite dipole [40,41],

$$w\left(\frac{r}{a}\right)=2\left(\frac{r}{a}\right)^{3}\left[\frac{1}{r/a}-\frac{1}{\sqrt{(r/a)^2+1}}\right], \tag{15}$$

$$v(r)=\frac{2}{a^2}\left[\frac{1}{r}-\frac{1}{\sqrt{r^2+a^2}}\right]. \tag{16}$$

(3) Modified dipole 1 [9,48],

$$w\left(\frac{r}{a}\right)=[(r/a)^{-2}+1]^{-3/2}, \tag{17}$$

$$v(r)=[r^2+a^2]^{-3/2}. \tag{18}$$

(4) Modified dipole 2

$$w\left(\frac{r}{a}\right)=[(r/a)^{-3}+1]^{-1}, \tag{19}$$

$$v(r)=[r^3+a^3]^{-1}. \tag{20}$$

(5) Modified dipole 3

$$w\left(\frac{r}{a}\right)=[(r/a)^{-1}+1]^{-3}, \tag{21}$$

$$v(r)=[r+a]^{-3}. \tag{22}$$

III. SCALING RELATIONS: PURE DOMAIN SHAPE FLUCTUATIONS

We consider the energetics of two domain configurations, a starting configuration, and another configuration which is identical in every way except that the domains are scaled by a factor b (Fig. 1). The original configuration is indicated by $b=1$, and the coupling constants, in lattice gas representation, that give rise to the original configuration are denoted as $J(1)$, $A(1)$, and $\mu(1)$. We seek coupling constants for the scaled system, $J(b)$, $A(b)$, and $\mu(b)$, for which the energy cost of fluctuations of the scaled domains is identical to the energy differences in the original system. Since we are examining the limit in which domain shapes fluctuate, but not the density within domains, the system energy is given in terms of integrals over the domain areas $\{\mathcal{D}_i\}$ and domain contours $\{\mathcal{C}_i\}$. The symbols $\{b\mathcal{D}_i\}$ and $\{b\mathcal{C}_i\}$ indicate the areas and contours of domains scaled by a factor b.

We begin by writing the Hamiltonian $\mathcal{H}_{LG}(b)$ for the scaled system in terms of domain contours and areas

$$\begin{aligned}\mathcal{H}_{LG}(b)/k_BT=&-\left[\mu(b)+\frac{q}{2}J(b)\right]\frac{1}{\sigma}\sum_i\int_{b\mathcal{D}_i}d\mathbf{r}+\gamma J(b)\\ &\times\sum_i\int_{b\mathcal{C}_i}dl+\sum_{i<j}\frac{A(b)}{\sigma^2}\int_{b\mathcal{D}_i}\int_{b\mathcal{D}_j}d\mathbf{r}d\mathbf{r}'\\ &\times|\mathbf{r}-\mathbf{r}'|^{-3}+\sum_i\frac{A(b)}{2\sigma^2}\\ &\times\int_{b\mathcal{D}_i}\int_{b\mathcal{D}_i}d\mathbf{r}d\mathbf{r}'\,w\left(\frac{|\mathbf{r}-\mathbf{r}'|}{a}\right)|\mathbf{r}-\mathbf{r}'|^{-3}.\end{aligned} \tag{23}$$

Terms that do not contain $w(|\mathbf{r}-\mathbf{r}'|/a)$ scale trivially

$$\int_{b\mathcal{D}_i}d\mathbf{r}=b^2\int_{\mathcal{D}_i}d\mathbf{r}, \tag{24}$$

$$\int_{b\mathcal{C}_i}dl=b\int_{\mathcal{C}_i}dl, \tag{25}$$

$$\int_{b\mathcal{D}_i}\int_{b\mathcal{D}_j}d\mathbf{r}d\mathbf{r}'|\mathbf{r}-\mathbf{r}'|^{-3}=b\int_{\mathcal{D}_i}\int_{\mathcal{D}_j}d\mathbf{r}d\mathbf{r}'|\mathbf{r}-\mathbf{r}'|^{-3}. \tag{26}$$

The intradomain repulsion term $E_{intra}(b)$, the last term on the right hand side of Eq. (23), contains the physically nontrivial scaling information. Following the same steps that give Eq. (26), the cutoff function in the intradomain repulsion term turns into $w(|\mathbf{r}-\mathbf{r}'|/(a/b))$, and the Hamiltonian for the scaled systems becomes

$$\begin{aligned}\mathcal{H}_{LG}(b)/k_BT=&-\left[\mu(b)+\frac{q}{2}J(b)\right]\frac{b^2}{\sigma}\sum_i\int_{\mathcal{D}_i}d\mathbf{r}+b\,\gamma J(b)\\ &\times\sum_i\int_{\mathcal{C}_i}dl+\sum_{i<j}\frac{bA(b)}{\sigma^2}\int_{\mathcal{D}_i}\int_{\mathcal{D}_j}d\mathbf{r}d\mathbf{r}'\\ &\times|\mathbf{r}-\mathbf{r}'|^{-3}+\sum_i\frac{bA(b)}{2\sigma^2}\\ &\times\int_{\mathcal{D}_i}\int_{\mathcal{D}_i}d\mathbf{r}d\mathbf{r}'\,w\left(\frac{|\mathbf{r}-\mathbf{r}'|}{a/b}\right)|\mathbf{r}-\mathbf{r}'|^{-3}.\end{aligned} \tag{27}$$

Eventually, we will match the coefficient of each area, contour, and dipole repulsion integral in the scaled Hamilton $\mathcal{H}_{LG}(b)$ to the corresponding coefficient in $\mathcal{H}_{LG}(1)$. At this point we can only make one match, the relation between

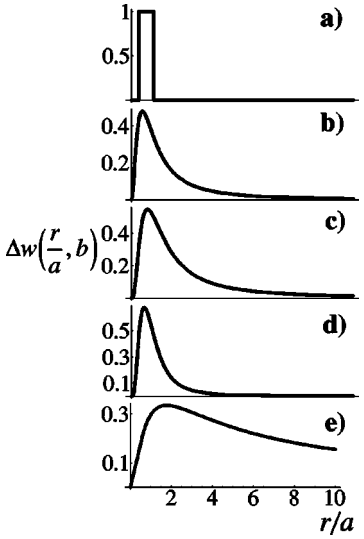

FIG. 3. Plots of $\Delta w(r/a,b)$, as defined in Eq. (29), for the five cutoff functions given in Sec. II C. A scale factor of $b=3$ is chosen for illustration. The function $\Delta w(r/a,b)$ vanishes for $r \gg a$, enabling the small domain curvature approximation made in Sec. III.

$A(b)$ and $A(1)$. If we demand that the interdomain repulsion in $\mathcal{H}_{LG}(b)$ be equal to the corresponding term in $\mathcal{H}_{LG}(1)$, then

$$bA(b)=A(1). \tag{28}$$

To make further progress, we have to tackle the more complicated intradomain repulsion term.

To relate $E_{intra}(b)$ to $E_{intra}(1)$, we cast the rescaled cutoff function in Eq. (27) in the following form, thereby defining a new function $\Delta w(|\mathbf{r}-\mathbf{r}'|/a,b)$,

$$w\left(\frac{|\mathbf{r}-\mathbf{r}'|}{a/b}\right)=w\left(\frac{|\mathbf{r}-\mathbf{r}'|}{a}\right)+\Delta w\left(\frac{|\mathbf{r}-\mathbf{r}'|}{a},b\right). \tag{29}$$

The function $\Delta w(r/a,b)$ is a short-range function of r, most prominent for $a/b<r<a$. The behavior of $\Delta w(r/a,b)$ for several cutoff functions is shown in Fig. 3.

The intradomain dipolar repulsion energy becomes

$$\begin{aligned}E_{intra}(b)&=\sum_i \frac{bA(b)}{2\sigma^2}\int_{\mathcal{D}_i}d\mathbf{r}\int_{\mathcal{D}_i}d\mathbf{r}'\,w\left(\frac{|\mathbf{r}-\mathbf{r}'|}{a}\right)|\mathbf{r}-\mathbf{r}'|^{-3}\\&\quad+\sum_i \frac{bA(b)}{2\sigma^2}\int_{\mathcal{D}_i}d\mathbf{r}\int_{\mathcal{D}_i}d\mathbf{r}'\,\Delta w\left(\frac{|\mathbf{r}-\mathbf{r}'|}{a},b\right)\\&\quad\times|\mathbf{r}-\mathbf{r}'|^{-3}\\&=E_{intra}(b=1)+\sum_i \frac{bA(b)}{2\sigma^2}\int_{\mathcal{D}_i}d\mathbf{r}\int_{\mathcal{D}_i}d\mathbf{r}'\\&\quad\times\Delta w\left(\frac{|\mathbf{r}-\mathbf{r}'|}{a},b\right)|\mathbf{r}-\mathbf{r}'|^{-3}.\end{aligned} \tag{30}$$

In the last step, we have substituted the relation of Eq. (28) and recognized the first term as $E_{intra}(b=1)$. We can rewrite the $\mathbf{r}'$ integral within $\mathcal{D}_i$ in the above equation as an integral over the entire system area minus an integral over values of $\mathbf{r}'$ that lie outside domain $\mathcal{D}_i$, which we denote by $\bar{\mathcal{D}}_i$.

$$\begin{aligned}E_{intra}(b)&=E_{intra}(b=1)+\sum_i \frac{bA(b)}{2\sigma^2}\int_{\mathcal{D}_i}d\mathbf{r}\int d\mathbf{r}'\\&\quad\times\Delta w\left(\frac{|\mathbf{r}-\mathbf{r}'|}{a},b\right)|\mathbf{r}-\mathbf{r}'|^{-3}-\sum_i \frac{bA(b)}{2\sigma^2}\\&\quad\times\int_{\mathcal{D}_i}d\mathbf{r}\int_{\bar{\mathcal{D}}_i}d\mathbf{r}'\,\Delta w\left(\frac{|\mathbf{r}-\mathbf{r}'|}{a},b\right)|\mathbf{r}-\mathbf{r}'|^{-3}.\end{aligned} \tag{31}$$

Consider the second term in the above equation. We define a new function

$$\begin{aligned}\Delta C_3(b)&\equiv\frac{1}{\sigma}\int d\mathbf{r}'\,\Delta w\left(\frac{|\mathbf{r}-\mathbf{r}'|}{a},b\right)\frac{a^3}{|\mathbf{r}-\mathbf{r}'|^3}\\&=\frac{2a^3\pi}{\sigma}\int_0^\infty dr\,r^{-2}\Delta w\left(\frac{r}{a},b\right).\end{aligned} \tag{32}$$

Because the cutoff functions depend on distance and cutoff parameter in the combination r/a, $\Delta C_3(b)$ evaluates to $(b-1)$ times a constant for each of the cutoffs defined in Sec. II C

$$\begin{aligned}\Delta C_3(b)&=\frac{2a^3\pi}{\sigma}\int_0^\infty dr\,r^{-2}\left[w\left(\frac{|\mathbf{r}-\mathbf{r}'|}{a/b}\right)-w\left(\frac{|\mathbf{r}-\mathbf{r}'|}{a}\right)\right]\\&=\frac{2a^2\pi}{\sigma}(b-1)\int_0^\infty dx\,x^{-2}w(x).\end{aligned} \tag{33}$$

Since $\Delta C_3(b)$ is independent of $\mathbf{r}$, the second term of $E_{intra}(b)$ in Eq. (31) becomes

$$\Delta C_3(b)\sum_i \frac{bA(b)}{2a^3\sigma}\int_{\mathcal{D}_i}d\mathbf{r}. \tag{34}$$

This term in the scaled system Hamiltonian $\mathcal{H}_{LG}(b)$ will contribute to the chemical potential when equated with the Hamiltonian $\mathcal{H}_{LG}(1)$ of the original system. The reason for the notation ''$\Delta C_3(b)$'' becomes apparent if we consider the continuum approximation to the lattice sum in Eq. (8),

$$C_3=\sum_{R'(R'\neq R)}\frac{a^3}{|R-R'|^3}\approx\frac{1}{\sigma}\int d\mathbf{r}'\,w\left(\frac{|\mathbf{r}-\mathbf{r}'|}{a}\right)\frac{a^3}{|\mathbf{r}-\mathbf{r}'|^3} \tag{35}$$

$$=\frac{1}{b^{-2}\sigma}\int d\mathbf{r}'\,w\left(\frac{|\mathbf{r}-\mathbf{r}'|}{a/b}\right)\frac{(a/b)^3}{|\mathbf{r}-\mathbf{r}'|^3}. \tag{36}$$

The second integral in the above equation repeats the continuum expression for the constant C_3, this time for a lattice

TABLE I. Integrals from five dipole cutoff functions introduced in Sec. II C that determine scaling properties. $\Delta C_3(b)$ and $G(b)$ are defined in Eqs. (32) and (41), respectively.

$w(R/a)$	Sharp cutoff	Finite dipole	Mod. dipole 1	Mod. dipole 2	Mod. dipole 3
$\Delta C_3(b)$	$(2\pi a^2/\sigma)(b-1)$	$(4\pi a^2/\sigma)(b-1)$	$(2\pi a^2/\sigma)(b-1)$	$(4\pi^2 a^2/(3\sqrt{3}\sigma))(b-1)$	$(\pi a^2/\sigma)(b-1)$
$G(b)$	$2\ln b$	$2\ln b$	$2\ln b$	$2\ln b$	$2\ln b$

constant a/b. Using both Eqs. (35) and (36) to interpret $\Delta C_3(b)$ as defined in Eq. (32), we find that

$$\Delta C_3(b) \approx (b-1) C_3 . \tag{37}$$

As shown in Table I, the five different cutoffs defined in Sec. II C produce coefficients of $(b-1)$ in $\Delta C_3(b)$ within a factor of order unity of each other and, as expected from Eq. (37), clustered about the exact lattice value of C_3 [27,28].

In the third term in Eq. (31), $\mathbf{r}$ must be within $\mathcal{D}_i$, $\mathbf{r}'$ lies outside $\mathcal{D}_i$, and yet $\Delta w(|\mathbf{r}-\mathbf{r}'|/a,b)$ is short ranged, as shown in Fig. 3. It follows that the major contribution to the this term comes from $\mathbf{r}$ and $\mathbf{r}'$ both near the domain contour $\mathcal{C}_i$. Now consider the integral over $\mathbf{r}'$ for fixed $\mathbf{r}$. If the radius of curvature of the contour is large compared to the lattice constant a, then over the range of $\mathbf{r}'$ where the integrand is nonzero, the contour is essentially straight. In a small domain curvature approximation, we use the coordinate system shown in Fig. 4. The location of $\mathbf{r}$ is specified by x, running along the contour, and y, the perpendicular distance from the contour. Similarly, the location of $\mathbf{r}'$ is specified by x' and y'. Within our small curvature approximation, the integral over x becomes an integral over the domain contour $\mathcal{C}_i$, and the remainder of the integral is independent of x. Therefore,

$$E_{intra}(b) = E_{intra}(b=1) + \sum_i \frac{bA(b)}{2a^3\sigma} \Delta C_3(b) \int_{\mathcal{D}_i} d\mathbf{r} - \sum_i \frac{bA(b)}{2\sigma^2} G(b) \int_{\mathcal{C}_i} dl, \tag{38}$$

where

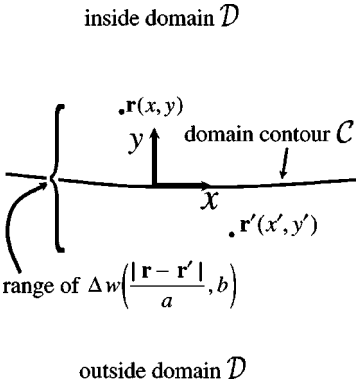

FIG. 4. Coordinate system used to evaluate the third term of Eq. (31).

$$G(b) = \int_0^\infty dy \int_{-\infty}^\infty dx' \int_{-\infty}^0 dy' \frac{\Delta w\left(\frac{\sqrt{x'^2-(y-y')^2}}{a},b\right)}{[x'^2-(y-y')^2]^{3/2}} \tag{39}$$

$$= \int_0^\infty dy \int_y^\infty dr r \int_{-\cos^{-1}(y/r)}^{\cos^{-1}(y/r)} d\phi \Delta w\left(\frac{r}{a},b\right) r^{-3}. \tag{40}$$

After performing the integral over ϕ, switching the order of integration over y and r and performing the r integration in closed form, we obtain

$$G(b) = 2\int_0^\infty dr r^{-1} \Delta w\left(\frac{r}{a},b\right). \tag{41}$$

$G(b)$ is equal to $2\ln b$ for any choice of the cutoff function that depends on the separation r through the combination r/a and is normalized so that $w(r/a)\to 1$ for large r. (The normalization is not really a restriction, since it can be imposed by a suitable redefinition of the coupling constant A.) The value of $G(b)$ is calculated by inserting the original definition (29) of $\Delta w(r/a,b)$ into Eq. (39), taking care to express the integral as a limit, since both terms below diverge separately

$$\begin{aligned} G(b) &= \lim_{R\to\infty} 2\int_0^R dr r^{-1}\left[w\left(\frac{r}{a/b}\right) - w\left(\frac{r}{a}\right)\right] \\ &= \lim_{R\to\infty} 2\left[\int_0^{bR/a} dx x^{-1} w(x) - \int_0^{R/a} dx x^{-1} w(x)\right] \\ &= \lim_{R\to\infty} 2\int_{R/a}^{bR/a} dx x^{-1} w(x). \end{aligned} \tag{42}$$

We can replace $w(x)$ by unity in the above expression because R is arbitrarily large

$$\begin{aligned} G(b) &= \lim_{R\to\infty} 2\int_{R/a}^{bR/a} dx x^{-1} \\ &= \lim_{R\to\infty} 2\left[\ln\left(b\frac{R}{a}\right) - \ln\left(\frac{R}{a}\right)\right] \\ &= 2\ln b. \end{aligned} \tag{43}$$

Since $G(b)$ is the same for a wide class of single-parameter cutoff functions and $\Delta C_3(b)$ differs by a constant of order unity, the derived energy scaling relations for the lattice gas acquire a general validity.

Substituting the result of Eq. (38) into the Hamiltonian of the scaled system, we obtain

$$\mathcal{H}_{LG}(b)/k_BT=-\left[\mu(b)+\frac{q}{2}J(b)\right]\frac{b^2}{\sigma}\sum_i\int_{\mathcal{D}_i}d\mathbf{r}+b\gamma J(b)\times\sum_i\int_{\mathcal{C}_i}dl+\sum_{i<j}\frac{bA(b)}{\sigma^2}\int_{\mathcal{D}_i}\int_{\mathcal{D}_j}d\mathbf{r}d\mathbf{r}'\times|\mathbf{r}-\mathbf{r}'|^{-3}+E_{intra}(b=1)+\Delta C_3(b)\times\sum_i\frac{bA(b)}{2a^3\sigma}\int_{\mathcal{D}_i}d\mathbf{r}-\sum_i G(b)\frac{bA(b)}{2\sigma^2}\int_{\mathcal{C}_i}dl. \tag{44}$$

All terms proportional to $\int_{\mathcal{C}_i}dl$ in the scaled system Hamiltonian $\mathcal{H}_{LG}(b)$ are equated with the surface tension in the original Hamiltonian $\mathcal{H}_{LG}(1)$, yielding a scaling relation for the attractive coupling constant,

$$J(b)=\frac{1}{b}J(1)+\frac{A(1)}{2b\gamma\sigma^2}G(b). \tag{45}$$

Knowing the scaling relations for $A(b)$ and $J(b)$, both of which are inversely proportional to the temperature, it is possible to deduce the scaling relation for the temperature-independent parameter $\eta(b)\equiv A(b)/J(b)$, the relative repulsion strength,

$$\frac{1}{\eta(b)}=\frac{1}{\eta(1)}+\frac{G(b)}{2\gamma\sigma^2}. \tag{46}$$

From the above equation, we express $G(b)$ in terms of $\eta(b)$

$$G(b)=2\gamma\sigma^2\left[\frac{1}{\eta(b)}-\frac{1}{\eta(1)}\right], \tag{47}$$

and using Eq. (43), we obtain an expression for the scaling parameter b in terms of $\eta(b)$

$$b=\exp\left\{\gamma\sigma^2\left[\frac{1}{\eta(b)}-\frac{1}{\eta(1)}\right]\right\}. \tag{48}$$

Combining the scaling relation for $\eta(b)$ and the result of the above equation, the scaling relation for $J(b)$ becomes

$$J(b)=J(1)\exp\left\{-\gamma\sigma^2\left[\frac{1}{\eta(b)}-\frac{1}{\eta(1)}\right]\right\}\frac{\eta(1)}{\eta(b)}. \tag{49}$$

In order to find the scaling relation for the chemical potential $\mu(b)$, we equate the coefficients of $\int_{\mathcal{D}_i}d\mathbf{r}$ before and after rescaling to obtain

$$-\left[\mu(1)+\frac{q}{2}J(1)\right]=-\left[\mu(b)+\frac{q}{2}J(b)\right]b^2+\Delta C_3(b)\frac{A(1)}{2a^3}. \tag{50}$$

Introducing $\delta\mu(b)$ from Eq. (5), the deviation of the chemical potential from its value at half coverage, and requiring that the continuum approximation be consistent with the definition of $\delta\mu(b)$ by invoking Eq. (37), we obtain a scaling relation for the chemical potential,

$$\delta\mu(b)=\frac{1}{b^2}\delta\mu(1). \tag{51}$$

We can transfer the scaling relations derived for the lattice gas to a spin system with the help of the relations of Eqs. (3)–(7). First we note that the parameter $\eta(b)$ is equivalent for both systems

$$\eta_{LG}(b)\equiv\frac{A(b)}{J(b)}=\frac{4A'(b)}{4J'(b)}\equiv\eta_{Is}(b)\equiv\eta(b). \tag{52}$$

The scaling relations for the spin Hamiltonian coupling constants $A'(b)$ and $J'(b)$ follow trivially,

$$A'(b)=b^{-1}A'(1), \tag{53}$$

$$J'(b)=J'(1)\exp\left\{-\gamma\sigma^2\left[\frac{1}{\eta(b)}-\frac{1}{\eta(1)}\right]\right\}\frac{\eta(1)}{\eta(b)}. \tag{54}$$

Through Eqs. (7) and (51), the scaling relation for the external field in the spin Hamiltonian is

$$h(b)=b^{-2}h(1). \tag{55}$$

IV. PREDICTIONS FROM THE SCALING RELATIONS

A. Scaling of the domain size and stripe melting temperature

The scaling theory creates a mapping from points on a phase diagram governed by relative repulsion strength $\eta(1)$ to points on the phase diagram governed by $\eta(b)$. This mapping links points in parameter space that exhibit identical domain behavior except for a change in overall domain length scale b. Points within the various phases as well as points at phase boundaries, are all mapped to new locations upon the scaling transformation. It suffices to follow the evolution of points at phase boundaries of the $\eta(1)$ phase diagram to determine the phase boundaries of the phase diagram for $\eta(b)$, so most of the ensuing discussion focuses on scaling of points at phase boundaries. For example, by mapping a system undergoing stripe melting (Fig. 2) at $\eta(1)$ to a system undergoing the same transition with rescaled stripes at $\eta(b)$, we find the dependence of the stripe melting point on the relative repulsion strength η.

Our scaling theory, in agreement with previous calculations [27,28,49–51] indicates that as the relative repulsion strength $\eta=A/J$ decreases, the domain size explodes more rapidly than exponentially [Eq. (48)]. This behavior is shown in Fig. 5. New predictions are obtained by considering the scaling behavior of the coupling constants precisely at the stripe melting point. Of particular interest is the stripe melting temperature as a function of η, $T_m(\eta)$. According to Eqs. (49) and (54), the stripe melting temperature $T_m(\eta)$

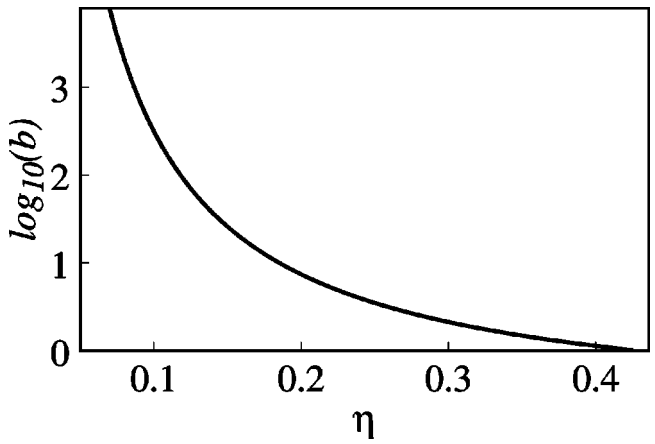

FIG. 5. The domain length scale b explodes more rapidly than exponentially with decreasing relative repulsion strength η, as illustrated by a plot of the scaling parameter b vs η.

rises with decreasing relative repulsion strength η (Fig. 6). Our preliminary comparison of Eq. (54) with numerical simulations exhibits excellent agreement [32]. The behavior of the stripe melting temperature predicted by Eqs. (49) or (54) also explains why a Langmuir monolayer has been observed to melt upon compression, as discussed in Sec. VI. While we focus on the scaling behavior of a system at the stripe melting point in Fig. 6, we emphasize that the scaling relations are applicable to any region of the phase diagram where the system configuration can be specified in terms of the domain shapes.

The theory of Sec. III is restricted to domain shape fluctuations in the absence of density fluctuations. Regimes of very small η [high $T_m(\eta)$], where magnetization (density) fluctuations become significant, must be considered separately. A modified version of our scaling theory that takes into account this feature is presented in Sec. V.

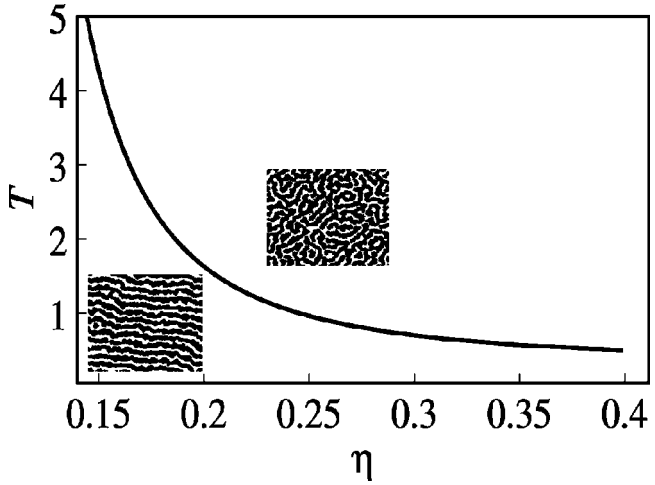

FIG. 6. Phase diagram for the Ising model with long-range repulsive interactions in the T-η plane as predicted by the scaling relations for temperature ($T=1/J$), Eq. (54), at the stripe melting point. Stripe melting temperature rises steeply as the relative repulsion strength $\eta=A/J$ decreases. Snapshots from simulations [32,52] are displayed to illustrate typical ordered and melted stripe configurations.

B. Temperature-magnetization or temperature-density phase diagrams

Previous numerical simulations [29–31] indicate that the stripe phase gives way to an isotropic bubble phase as the magnetization becomes nonzero in spin lattice models, or coverage departs from 1/2 in the lattice gas. The T-h or T-μ phase diagram exhibits an isotropic/stripe coexistence line in the shape of a dome. The zero-field or half-coverage stripe melting point is located at the top of the dome. The interior of the dome is a stripe phase with twofold order (not a coexistence region), which may appear similar to Fig. 2(a). Outside the dome is an isotropic phase, either melted stripes above the dome [Fig. 2(b)] or bubbles (possibly elongated) on either side [Fig. 2(c) and 2(d)]. Mean-field theory [19,26] and the self-consistent field theory of Brazovskii [24] also predict an isotropic/stripe coexistence line in the shape of a dome.

If the shape of the isotropic/stripe coexistence line is known from theory or experiment at one relative repulsion strength η, then the scaling theory of Sec. III makes useful predictions about the coexistence curve at other values of η. For lack of more definite input from theory or experiment, we choose an arbitrary two-parameter form of the coexistence curve to illustrate the scaling relations derived in Sec. III. Adopting the spin representation and letting $T_m(h)$ stand for the stripe/isotropic transition temperature as a function of h, that is, the coexistence curve, we consider the simple power relation,

$$|T_m(h=0)-T_m(h)|^{\zeta}=C\tanh(h). \tag{56}$$

Several values of the exponent ζ were explored. The constant C was chosen to reproduce simulation data at the value of η we adopted for $b=1$. Equations (51) and (55) predict the scaling behavior of the chemical potential or external magnetic field, respectively. Combining these results with the scaling relation for temperature, Eqs. (49) and (54), we can predict how the coexistence curve evolves as η is modified. Phase diagrams for several chosen values of the exponent ζ and a range of η's are shown in Fig. 7, all exhibiting similar qualitative behavior: as η decreases, the top of the dome rises because the stripe melting temperature at zero field increases, as discussed in Sec. IV A. However, the width of the stripe phase portion of the phase diagram shrinks as a consequence of Eq. (55), which indicates that the field h decreases upon scaling to larger domain length scales. The behavior predicted by Eq. (55) will be tested against computer simulations in a forthcoming work [52].

V. HIGH TEMPERATURE PHENOMENOLOGICAL THEORY

The scaling relations discussed until this point assume that the temperature remains sufficiently low so that only domain shapes fluctuate, but not the magnetization or density within domains. The range of validity of the pure shape fluctuation theory is extensive, including all regions of the phase

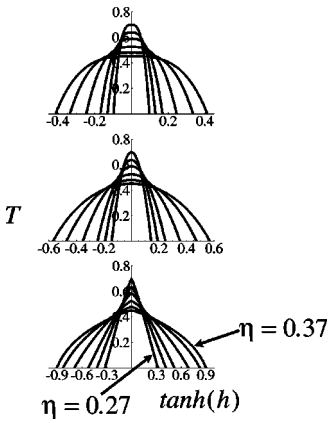

FIG. 7. Qualitative phase diagrams in the T-tanh h plane obtained by scaling the stripe-isotropic coexistence curve, Eq. (56). This curve is chosen for purpose of illustration. The same trends are obtained for three different values of the exponent ζ, $\frac{1}{3}$ (top), $\frac{1}{2}$ (middle), and $\frac{5}{6}$ (bottom), which give domes flatter than parabolic, parabolic, and steeper than parabolic, respectively. The coexistence curves are drawn for the sequence of η values 0.270, 0.285, 0.300, 0.325, 0.350, and 0.370. The placement of curves for the different η in all three panels is as indicated for the bottom panel.

diagram which, so far, are amenable to computer simulation [29,32]. However, it is of interest to speculate as to what may occur when the temperature is sufficiently high to permit patches of overturned spins, or in lattice gas language, vacancies in the majority phase and appreciable vapor pressure in the minority phase. We expect density fluctuations to occur simultaneously with shape fluctuations when the temperature begins to approach the critical temperature of the Ising model without repulsions. This is a considerably more complicated situation, and we do not have a detailed theory for coupled domain shape and density fluctuations in the high-temperature region.

In this section we explore the effects of density fluctuations in a phenomenological way. Rather than truly coupling domain shape and density fluctuations, (speaking now in lattice gas language) we assume that the densities of the minority component ($\langle n\rangle_1$ inside domains) and majority component ($\langle n\rangle_0$ between domains) each vary with temperature as if they were part of *hypothetical uniform phases* in coexistence, and eventually coalesce as the temperature reaches a critical value associated with the hypothetical uniform phases. Approximating the density fluctuations within and outside of domains as though they were characteristic of uniform phases is motivated by the steep rise in domain size and stripe melting temperature as η decreases. This approximation will cease to be valid when the correlation length for density fluctuations becomes comparable to the domain length scale.

As the critical point of the hypothetical uniform phases is approached from below,

$$\Delta n \equiv \langle n\rangle_1 - \langle n\rangle_0 \propto t^{\beta}, \quad t \equiv \frac{T_c - T}{T_c} = \frac{J - J_c}{J}. \tag{57}$$

Before proceeding further we note that T_c or J_c, the critical parameters of hypothetical coexisting uniform phases, are themselves functions of η because the presence of repulsions will serve to decrease T_c. This can be seen including both attractive and repulsive interactions in the effective field h_{eff} within Curie-Weiss theory

$$m = \tanh(h + h_{eff}), \tag{58}$$

$$h_{eff} = (qJ' - A'C_3/a^3)m = J'(q - \eta C_3/a^3)m. \tag{59}$$

According to Eq. (58), increasing η produces a linear decrease in the critical temperature

$$T_c(\eta) = \frac{1}{J_c(\eta)} = q\left(1 - \frac{C_3\eta}{qa^3}\right). \tag{60}$$

We do not expect Eq. (60) to be very accurate, so below we adopt the linear dependence of T_c on η but explore different values of the linear coefficient. In the following, note the distinction between T_m, the stripe melting temperature, and T_c, the temperature at which the magnetization (density) difference vanishes between majority and minority phases, treated as hypothetical uniform phases. The depression of the critical point with increasing repulsion has been previously predicted by Pini *et al.* [53] for a three-dimensional hard sphere fluid with Yukawa-type attractive interactions and an additional Yukawa-type repulsion. Their calculations were appropriate for a uniform system in the absence of domains.

A. Scaling relations in the presence of density fluctuations

Since our energy expression will become more complex than in Sec. III, we maintain simplicity by not considering the external field or chemical potential here. This has no effect on the scaling relations we derive for J and A and is equivalent to working in a constant magnetization or constant particle number ensemble, in which case we can omit terms proportional to $\Sigma_R s_R$ or $\Sigma_R n_R$. Besides the densities, $\langle n\rangle_1$ and $\langle n\rangle_0$, fluctuations within domains also change the surface tension. We expect that the surface tension is controlled by the distance from the critical point t introduced in Eq. (57), which in turn depends upon the scaling parameter b: $\gamma = \gamma(t(b))$. The Hamiltonian for the lattice gas allowing for density fluctuations is given by

$$H_{LG}(1)/k_BT = J(1)\gamma(1)\sum_i \int_{C_i} dl + \frac{A(1)}{\sigma^2}[\Delta n(1)]^2 \times\left[\sum_{i<j}\int_{\mathcal{D}_i}\int_{\mathcal{D}_j} d\mathbf{r}d\mathbf{r}' v(|\mathbf{r}-\mathbf{r}'|) + \frac{1}{2}\sum_i \int_{\mathcal{D}_i}\int_{\mathcal{D}_i} d\mathbf{r}d\mathbf{r}' v(|\mathbf{r}-\mathbf{r}'|)\right]. \tag{61}$$

The interdomain and intradomain dipole repulsion energies, in square brackets, are obtained by subtracting a uniform background of density $\langle n\rangle_0$. Working at fixed overall magnetization or density, this contributes a constant to the energy. The configuration-dependent part of the dipole repul-

sion energy depends on the *difference* in densities, Δn, of the minority and majority components.

Following the same approach as in Sec. III, we introduce $v(r)=w(r/a)r^{-3}$ in the above Hamiltonian and substitute $w(r/a)\to 1$ in the interdomain dipolar repulsion term

$$H_{LG}(1)/k_BT=J(1)\gamma(1)\sum_i \int_{C_i} dl+\frac{A(1)}{\sigma^2}[\Delta n(1)]^2 \times\left[\sum_{i<j}\int_{\mathcal{D}_i}\int_{\mathcal{D}_j} d\mathbf{r}d\mathbf{r}'|\mathbf{r}-\mathbf{r}'|^{-3} +\frac{1}{2}\sum_i \int_{\mathcal{D}_i}\int_{\mathcal{D}_i} d\mathbf{r}d\mathbf{r}' w\left(\frac{|\mathbf{r}-\mathbf{r}'|}{a}\right)|\mathbf{r}-\mathbf{r}'|^{-3}\right]. \tag{62}$$

We rescale the system by a factor b

$$H_{LG}(b)/k_BT=bJ(b)\gamma(b)\sum_i \int_{C_i} dl+\frac{bA(b)}{\sigma^2}[\Delta n(b)]^2 \times\left[\sum_{i<j}\int_{\mathcal{D}_i}\int_{\mathcal{D}_j} d\mathbf{r}d\mathbf{r}'|\mathbf{r}-\mathbf{r}'|^{-3} +\frac{1}{2}\sum_i \int_{\mathcal{D}_i}\int_{\mathcal{D}_i} d\mathbf{r}d\mathbf{r}' w\left(\frac{|\mathbf{r}-\mathbf{r}'|}{a/b}\right)|\mathbf{r}-\mathbf{r}'|^{-3}\right]. \tag{63}$$

The scaling relation for $A(b)$ is obtained by equating the coefficients of the interdomain dipolar repulsion terms before [Eq. (62)] and after [Eq. (63)] rescaling,

$$A(1)=bA(b)\left[\frac{\Delta n(b)}{\Delta n(1)}\right]^2. \tag{64}$$

This reduces to our low-temperature result of Eq. (28) when we set $\langle n\rangle_1=1$, $\langle n\rangle_0=0$.

To find a temperature-dependent scaling relation for $J(b)$, we compare the coefficients of the surface tension terms before and after rescaling,

$$\frac{1}{b}J(1)\gamma(1)=J(b)\gamma(b)-\frac{A(b)}{2\sigma^2}G(b)[\Delta n(b)]^2, \tag{65}$$

which gives

$$J(b)\gamma(b)=\frac{1}{b}J(1)\gamma(1)+\frac{G(b)}{2\sigma^2 b}[\Delta n(1)]^2A(1). \tag{66}$$

The above results imply the following scaling relation for the relative repulsion strength η,

$$\frac{1}{\eta(b)}\frac{\gamma(b)}{[\Delta n(b)]^2}=\frac{1}{\eta(1)}\frac{\gamma(1)}{[\Delta n(1)]^2}+\frac{G(b)}{2\sigma^2}. \tag{67}$$

Introducing $G(b)=2\ln(b)$ in the above expression, we obtain a high-temperature phenomenological expression for b,

$$b=\exp\left\{\frac{\sigma^2\gamma(b)}{\eta(b)[\Delta n(b)]^2}-\frac{\sigma^2\gamma(1)}{\eta(1)[\Delta n(1)]^2}\right\}. \tag{68}$$

We substitute the above results into Eq. (66) to obtain the scaling relation for $J(b)$,

$$J(b)=J(1)\frac{1}{b}\frac{\eta(1)}{\eta(b)}\left[\frac{\Delta n(b)}{\Delta n(1)}\right]^2, \tag{69}$$

which reduces to the low-temperature result of Eq. (54) when $\langle n\rangle_1=1$, $\langle n\rangle_0=0$.

B. Consequences of density fluctuations

Expressions (67) and (69) give a system of equations that predict the stripe melting temperature as a function of η into the region where density fluctuations begin to be significant, but not beyond the point where the correlation length approaches the domain size b. To obtain explicit expressions we require $\Delta n(t)$ and $\gamma(t)$, which, for lack of better input, we estimate using exact solutions for the Ising model. This gives the correct low-temperature limits of $\Delta n(t)$ and $\gamma(t)$, and the correct scaling behavior as $T\to T_c(\eta)$, or equivalently $t\to 0$. Since our numerical simulations were performed for the triangular lattice, we used the corresponding analytic expressions [54,55] although the choice of lattice makes no qualitative difference. Recall that, based on mean-field estimates, we expect $T_c(\eta)$ to be a linearly decreasing function of η [Eq. (60)]. By comparison with our numerical simulations [32] we know that the mean-field estimate, Eq. (60), predicts a far too drastic decrease of T_c with η. Therefore, we adopt the form

$$T_c(\eta)=T_c(0)[1-\alpha\eta], \tag{70}$$

where $T_c(0)$ is the critical temperature of the bare Ising model at $\eta=0$. Since we observe virtually no density fluctuations in regions of the phase diagram accessible to simulations, we can put an approximate upper bound on α, which turns out to be $\alpha\lesssim 1.75$ for the triangular lattice.

Using the Ising model estimates for the behavior of $\Delta n(t)$ and $\gamma(t)$, we find that density fluctuations suppress the growth of the domain length scale with decreasing η, as exhibited in Fig. 8(a). This trend stems from the different critical exponents for the two quantities, $\Delta n(t)\sim t^{1/8}$ and $\gamma(t)\sim t^1$. Hence density fluctuations cause domain wall energy to vanish more rapidly than the repulsive energy, therefore allowing smaller domain size than in the absence of density fluctuations. Tracking the evolution of the domain length scale with temperature at fixed η, we see that the domains shrink as temperature is increased, as shown in Fig. 8(b). This effect at fixed η was first described theoretically by Keller and McConnell [56], who also confirmed the effect in experiments on a Langmuir monolayer. Whether or not the shrinkage of domains is observed below the stripe melting temperature depends on the value of η. For larger η, $T_m\ll T_c$, density fluctuations will still be negligible near T_m

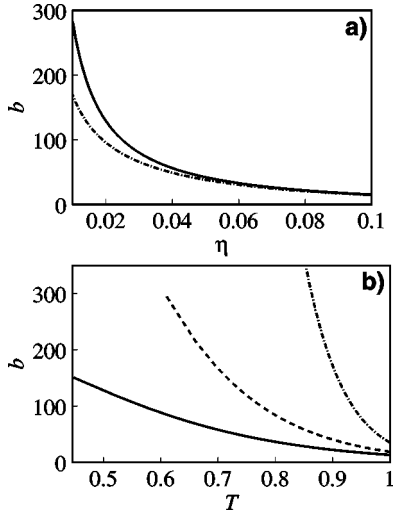

FIG. 8. (a) Scaling of the parameter b as a function of η, accounting for magnetization (density) fluctuations within domains according to the phenomenological theory of Sec. V (dot-dashed curve) and without fluctuations (solid curve). (b) Domain length scale b as a function of temperature at fixed η. The contraction of the domain size with temperature is shown for $\eta=0.1$ (solid curve), $\eta=0.08$ (dashed curve), and $\eta=0.05$ (dot-dashed curve) assuming that at $\eta=0.37$, as expected (and observed in simulations [29,32,52]) for larger η, the domain length scale is independent of temperature below T_m. The data show that systems at smaller values of η show the strongest temperature dependence. The parameter α in Eq. (70) is taken to be 1.75 in these calculations.

and virtually no change in domain size with temperature below T_m will occur. Alternatively, when T_m approaches T_c there will be noticeable shrinkage with increasing temperature below T_m. This effect is discussed further in the concluding section.

It is useful to be cognizant of the behavior of our expressions in the limit of vanishing η, even though they lose their physical validity before η reaches zero, when the correlation length ξ of density fluctuations becomes comparable to the domain length scale predicted by Eq. (68). In the small η limit, if $\Delta n \sim t^{\beta}$, then Eqs. (67), (69), and (70) predict that

$$\eta \propto t^{2\beta} \quad (\text{small } \eta). \tag{71}$$

As a consequence, the exponent in Eq. (68) has the following small η behavior:

$$\frac{\gamma(t)}{\eta[\Delta n(t)]^2} \sim t^{1/2}. \tag{72}$$

According to Eqs. (67), (69), and (70) b is finite at $\eta=0$, whereas it strongly diverges in the absence of density fluctuations. While our phenomenological theory can be trusted to predict that density fluctuations cause an initial deviation of b toward smaller values, the theory is not valid all the way to $\eta=0$. Possible implications of the small η behavior are discussed in the concluding section.

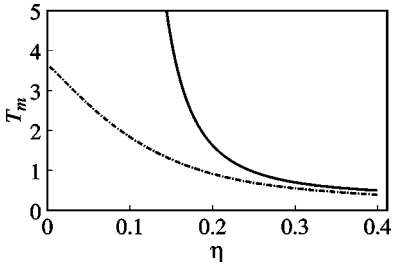

FIG. 9. Scaling of the stripe melting temperature as a function of η in the cases of no magnetization (density) fluctuations within domains (solid curve), and magnetization (density) fluctuations within domains as described by the phenomenological theory of Sec. V (dot-dashed curve). The parameter α in Eq. (70) is taken to be 1.75 in these calculations.

Density fluctuations also suppress the stripe melting temperature. T_m with and without density fluctuations are compared in Fig. 9. This effect, like the suppression of the domain length scale b, is driven by the fact that γ decreases more rapidly than Δn with the onset of density fluctuations. As a result, the *effective* η, a ratio of repulsions ($\propto \Delta n^2$) to attractions ($\propto \gamma$), is larger than the actual η in the presence of density fluctuations. One can understand the behavior of T_m in Fig. 9 as a modification of Fig. 7 in which the points are pulled to effective η values that are larger than the actual η values.

VI. DISCUSSION

Despite the relative simplicity of the dipolar Ising model and analogous continuum models, they exhibit a rich variety of physical behavior. The phase diagram and the elementary excitations that govern its phase transitions are not completely understood at present. Together with large-scale simulations [32], the scaling theory presented in this work begins to organize at least some of the behavior of these models with competing attractions and dipolar repulsions, particularly the phase diagram at larger relative repulsion strength $\eta=A/J$. Here the stripe melting temperature is well below the bare Ising model critical temperature and density fluctuations within domains are infrequent. The scaling theory derived in Sec. III of this work predicts how the stripe melting temperature will vary with η. We have already made a preliminary comparison with numerical results [32] and in a forthcoming publication will make a more extensive check of the theory, including the predictions about nonzero fields [52].

Some of the phase diagram is known to be sensitive to details of the cutoff functions used at short range for the r^{-3} repulsive potential and, in continuum models, to precisely how the line tension is treated [27,28]. An example is the bubble to stripe phase transition at low temperature [27,28,57,58]. However, the family of results we derive here through scaling relations will be insensitive to these details. When the domain radius of curvature is much larger than the microscopic cutoff length, we showed in Sec. III that the scaling relations are insensitive to the precise form of the cutoff function $w(r/a)$. This is reflected in the behavior of

the functions $G(b)$, which is completely independent of $w(r/a)$, and $\Delta C_3(b)$, which depends on $w(r/a)$ only through a constant prefactor. Hence, one of the predictions of our work is that the scaling relations should be obeyed by a variety of physical systems so long as they are governed by short-ranged attractions and long-ranged r^{-3} repulsions.

Our scaling theory explains the otherwise perplexing experimental observation [38] that stripe melting in a Langmuir monolayer is induced by compression. Compressing the monolayer increases the surface dipole density and therefore increases the parameter *A*. The magnitude of attractions between surfactants in the monolayer, characterized by *J*, would be expected to remain unaffected or possibly even decrease if neighboring surfactants are driven from their equilibrium separation by the compression. Hence compression effectively increases the relative repulsion strength η. On the phase diagram of Fig. 6, increasing η at constant temperature drives the system from the stripe phase (lower left of the figure) across the melting line to the isotropic phase (upper right).

The last section of this work explores the small η behavior of the dipolar Ising model in a phenomenological way. The hallmark of the small η regime is the increase in the stripe melting temperature to the point where it is a significant fraction of the bare Ising model critical temperature. Now spin fluctuations (overturned spins) within domains will start to play a role. Our phenomenological theory treats the magnetization (or, in lattice gas language, density) within the domains as if they were that of hypothetical coexisting uniform phases in the absence of domain formation. This approach will be successful when the correlation length ξ for magnetization or density fluctuations within domains is much less than the width *b* of the domains. We can therefore predict that the stripe melting temperature and domain width will be suppressed by spin fluctuations at the *onset* of spin fluctuation effects. The physical origin for the suppression of the domain width by fluctuations, as first noted by Keller and McConnell [56], is clear: surface tension decreases more rapidly than the magnetization or density difference between majority and minority phases as a critical point is approached. The system will accommodate more total domain boundary length, and thus smaller domains in the presence of fluctuations within domains.

The situation is less clear when η becomes small, and the stripe melting temperature rises to the point where ξ approaches *b*, that is, when the correlation length for spin fluctuations becomes comparable to the domain width. The theory of Sec. V A predicts that the domain width is suppressed by fluctuations, and when carried past its region of validity to very small η, predicts that the domain width *b* remains finite for all η. An interesting cross over will occur if higher levels of theory or more extensive simulations confirm that *b* remains finite or diverges less rapidly than ξ as $\eta \to 0$. If ξ increases to the magnitude of *b* then a transition from twofold stripe order to an isotropic phase, driven by overturned spins within domains, will preempt the defect-meditated stripe melting observed for higher values of η in our simulations [32]. In other words, the mechanism and nature of the stripe melting transition will change at a certain crossover value of η. We speculated about this possibility in our previous work, where a tentative phase diagram is given [32].

There is another consequence of the theory of Sec. V that may be quite amenable to experimental test. Since the domain length scale *b* is suppressed by density fluctuations, we expect that domains, if allowed to equilibrate, will shrink as the temperature is raised at constant η. At low temperature, spin or density fluctuations are negligible and the domain length scale will be given by the pure shape fluctuation theory of Sec. III. Then as fluctuations within domains are excited at higher temperatures, *b* will instead be given by the smaller value predicted by the shape *and* magnetization/density fluctuation theory of Sec. V. This trend presupposes that temperature has no other effect on the system besides domain shape and magnetization/density fluctuations. If, for example, increasing temperature caused a change in molecular orientation within a Langmuir monolayer, the consequences for domain size could be more complicated. Another caveat is that the system must be in equilibrium. The effect may not be observed if exchange of particles between domains is slow and domains remain at a metastable size.

In this work, we have shown that a scaling theory built on a continuum treatment of a spin or lattice gas model with long-range dipolar repulsions is capable of predicting many features of the phase diagram. The theory should be applicable to a wide range of systems because, even though the dipolar interactions require a short-range cutoff, the important scaling relations are independent of the precise nature of the cutoff function. While many features of the dipolar spin model are now understood, the region of the phase diagram in the limit of vanishing repulsion strength remains a challenging area for future investigations.

ACKNOWLEDGMENTS

Acknowledgment is made to the donors of The Petroleum Research Fund, administered by the ACS, for support of this research and to the Ohio Supercomputer Center for computational resources.

[1] M. Seul and D. Andelman, Science **267**, 476 (1995).

[2] C. Kittel, Phys. Rev. **70**, 965 (1946); C. Kooy and U. Enz, Philips Res. Rep. **15**, 7 (1960); A. A. Thiele, J. Appl. Phys. **41**, 1139 (1970); W. A. Barker and G. A. Gehring, J. Phys. C **16**, 6415 (1983); R. E. Rosensweig, M. Zahn, and R. Shumovich, J. Magn. Magn. Mater. **39**, 127 (1983).

[3] M. Seul and R. Wolfe, Phys. Rev. A **46**, 7519 (1992).

[4] R. M. Weis and H. M. McConnell, Nature (London) **310**, 47 (1984).

[5] R. M. Weis and H. M. McConnell, J. Phys. Chem. **89**, 4453 (1985).

[6] W. M. Heckl and H. Möhwald, Ber. Bunsenges. Phys. Chem.

90, 1159 (1986).
[7] M. Lösche and H. Möhwald, J. Colloid Interface Sci. **131**, 56 (1989).
[8] H. Möhwald, Thin Solid Films **159**, 1 (1988).
[9] H. M. McConnell, Annu. Rev. Phys. Chem. **42**, 171 (1991).
[10] K. Kern, H. Niehus, A. Schatz, P. Zeppenfeld, J. Goerge, and G. Comsa, Phys. Rev. Lett. **67**, 855 (1991).
[11] J. H. Weaver, Nav. Res. Rev. **43**, 16 (1991).
[12] H. Hörnis, J. R. West, E. H. Conrad, and E. Elliatioğlu, Phys. Rev. B **47**, 13 055 (1993).
[13] S. Müller, P. Bayer, C. Reischl, K. Heinz, B. Feldmann, H. Zillgen, and M. Wuttig, Phys. Rev. Lett. **74**, 765 (1995).
[14] C. M. Knobler and D. K. Schwartz, Curr. Opin. Colloid Interface Sci. **4**, 46 (1999).
[15] J. K. Cox, A. Eisenberg, and R. B. Lennox, Curr. Opin. Colloid Interface Sci. **4**, 52 (1999).
[16] R. Wang, A. N. Parikh, J. D. Beers, A. P. Shreve, and B. Swanson, J. Phys. Chem. B **103**, 10 149 (1999).
[17] S. H. Choi, K. L. Wang, M. S. Leung, G. W. Stupian, N. Preser, S. W. Chung, G. Markovich, S. H. Kim, and J. R. Heath, J. Vac. Sci. Technol. **B17**, 1425 (1999).
[18] C. M. Knobler and R. C. Desai, Annu. Rev. Phys. Chem. **43**, 207 (1992).
[19] D. Andelman, F. Broçhard, and J.-F. Joanny, J. Chem. Phys. **86**, 3673 (1987).
[20] M. Seul and M. J. Sammon, Phys. Rev. Lett. **64**, 1903 (1990).
[21] O. L. Alerhand, D. Vanderbilt, R. D. Meade, and J. D. Joannopoulos, Phys. Rev. Lett. **61**, 1973 (1988).
[22] D. Vanderbilt, O. L. Alerhand, R. D. Meade, and J. D. Joannopoulos, J. Vac. Sci. Technol. B **7**, 1013 (1989).
[23] D. Vanderbilt, Surf. Rev. Lett. **4**, 811 (1997).
[24] S. A. Brazovskiĭ, Zh. Eksp. Teor. Fiz. **68**, 175 (1975) [Sov. Phys. JETP **41**, 85 (1975)].
[25] J. Toner and D. R. Nelson, Phys. Rev. B **23**, 316 (1981).
[26] T. Garel and S. Doniach, Phys. Rev. B **26**, 325 (1982).
[27] M. M. Hurley and S. J. Singer, J. Phys. Chem. **96**, 1938 (1992).
[28] M. M. Hurley and S. J. Singer, J. Phys. Chem. **96**, 1951 (1992).
[29] M. M. Hurley and S. J. Singer, Phys. Rev. B **46**, 5783 (1992).
[30] I. Booth, A. B. MacIsaac, J. P. Whitehead, and K. De'Bell, Phys. Rev. Lett. **75**, 950 (1995).
[31] J. Arlett, J. P. Whitehead, A. B. MacIsaac, and K. De'Bell, Phys. Rev. B **54**, 3394 (1996).
[32] A. D. Stoycheva and S. J. Singer, Phys. Rev. Lett. **84**, 4657 (2000).
[33] J. M. Kosterlitz and D. J. Thouless, Prog. Low Temp. Phys. **7B**, 373 (1978).
[34] D. J. Thouless, Phys. Rep. **13**, 93 (1974).
[35] J. M. Kosterlitz, J. Phys. C **7**, 1046 (1974).
[36] J. M. Kosterlitz and D. J. Thouless, J. Phys. C **6**, 1181 (1973).
[37] J. M. Kosterlitz and D. J. Thouless, J. Phys. C **5**, 124 (1972).
[38] M. Seul and V. S. Chen, Phys. Rev. Lett. **70**, 1658 (1993).
[39] Animations of our simulations of an Ising model with additional dipolar repulsions can be viewed at http://chemistry.ohio-state.edu/~singer/DipolarIsingSimulations.
[40] P. Muller and F. Gallet, J. Phys. Chem. **95**, 3257 (1991).
[41] D. P. Jackson, R. E. Goldstein, and A. O. Cebers, Phys. Rev. E **50**, 298 (1994).
[42] R. Kretschmer and K. Binder, Z. Phys. B **34**, 375 (1979).
[43] M. A. Mayer and T. K. Vanderlick, Phys. Rev. E **55**, 1106 (1997).
[44] R. K. Kalia and P. Vashishta, J. Phys. C **14**, L643 (1981).
[45] D. Levesque, G. N. Patey, and J. J. Weis, Mol. Phys. **34**, 1077 (1977).
[46] G. N. Patey, D. Levesque, and J. J. Weis, Mol. Phys. **45**, 733 (1982).
[47] M. E. van Leeuwen and B. Smit, Phys. Rev. Lett. **71**, 3991 (1993).
[48] H. M. McConnell and R. de Koker, J. Phys. Chem. **96**, 6820 (1992).
[49] H. M. McConnell, D. Keller, and H. Gaub, J. Phys. Chem. **90**, 1717 (1986).
[50] D. J. Keller, H. M. McConnell, and V. T. Moy, J. Phys. Chem. **90**, 2311 (1986).
[51] H. M. McConnell, Proc. Natl. Acad. Sci. U.S.A. **86**, 3452 (1989).
[52] A. D. Stoycheva and S. J. Singer (unpublished).
[53] D. Pini, G. Jialin, A. Parola, and L. Reatto, Chem. Phys. Lett. **327**, 209 (2000).
[54] L. Onsager, Phys. Rev. **65**, 117 (1944).
[55] P. G. Watson, Proc. Phys. Soc. London **91**, 940 (1967).
[56] S. L. Keller and H. M. McConnell, Phys. Rev. Lett. **82**, 1602 (1999).
[57] T. C. Halsey, Phys. Rev. **48**, R673 (1993).
[58] K.-O. Ng and D. Vanderbilt, Phys. Rev. B **52**, 2177 (1995).